The Most Metal-Rich Intervening Quasar Absorber Known[⋆]

C. Péroux[1], V. P. Kulkarni[2], J. Meiring[2], R. Ferlet[3], P. Khare[4], J. T. Lauroesch[5], G. Vladilo[6], & D. G. York[7].

[1] European Southern Observatory, Garching-bei-München, Germany. e-mail: `cperoux@eso.org`

[2] Dept. of Physics and Astronomy, Univ. of South Carolina, Columbia, USA.

[3] Institut d'Astrophysique de Paris, UMR7095 CNRS, Universite Pierre & Marie Curie, France.

[4] Dept. of Physics, Utkal University, Bhubaneswar, India.

[5] Dept. of Physics and Astronomy, Northwestern University, Evanston, USA.

[6] Osservatorio di Trieste, Trieste, Italy.

[7] Dept. of Astronomy and Astrophysics, Univ. of Chicago, Chicago, USA.

Abstract. The metallicity in portions of high-redshift galaxies has been successfully measured thanks to the gas observed in absorption in the spectra of quasars, in the Damped Lyman-α systems (DLAs). Surprisingly, the global mean metallicity derived from DLAs is about $1/10^{th}$ solar at $0 \lesssim z \lesssim 4$ leading to the so-called "missing-metals problem". In this paper, we present high-resolution observations of a sub-DLA system at z_{abs}=0.716 with super-solar metallicity toward SDSS J1323−0021. This is the highest metallicity intervening quasar absorber currently known, and is only the second super-solar absorber known to date. We provide a detailed study of this unique object from VLT/UVES spectroscopy. We derive [Zn/H]=+0.61, [Fe/H]=−0.51, [Cr/H]=< −0.53, [Mn/H] = −0.37, and [Ti/H] = −0.61. Observations and photoionisation models using the CLOUDY software confirm that the gas in this sub-DLA is predominantly neutral and that the abundance pattern is probably significantly different from a Solar pattern. Fe/Zn and Ti/Zn vary among the main velocity components by factors of ∼ 3 and ∼ 35, respectively, indicating non-uniform dust depletion. Mn/Fe is super-solar in almost all components, and varies by a factor of ∼ 3 among the dominant components. It would be interesting to observe more sub-DLA systems and determine whether they might contribute significantly toward the cosmic budget of metals.

Key words. Galaxies: abundances – intergalactic medium – quasars: absorption lines – quasars: individual: SDSS J1323−0021

1. Introduction

Damped Lyman-α systems (DLAs) seen in absorption in the spectra of background quasars are selected over all redshifts independent of the intrinsic luminosities of the underlying galaxies. They have hydrogen column densities, $\log N_{HI} \gtrsim 20.3$ and are the major contributors to the neutral gas in the Universe at high redshifts (Storrie-Lombardi & Wolfe 2000; Péroux et al. 2003b). But it has been suggested that at least some of the H I lies in systems with H I column density below that required by the traditional DLA definition, in the "sub-Damped Lyman-α Systems (sub-DLAs)" with $19.0 < \log N_{HI} < 20.3$. The DLAs and sub-DLAs offer direct probes of element abundances over > 90% of the age of the Universe. Zn is a good probe of the total (gas and solid phase) metallicity, in DLAs because Zn tracks Fe in most Galactic stars with [Fe/H]> −3, it is undepleted on interstellar dust grains, and the lines of the dominant ionisation species Zn II are often unsaturated (e.g., Pettini et al. 1999). Abundances of depleted elements such as Cr or Fe rel-

ative to Zn probe the dust content and the relative abundances can also yield information about the nucleosynthetic processes (e.g., Pettini et al. 1997; Kulkarni, Fall, & Truran, 1997; Péroux et al., 2002; Khare et al. 2004). A study of the cosmological evolution of the H I column density-weighted mean metallicity in DLAs (e.g., Kulkarni & Fall, 2002) shows surprising results. Contrary to most models of cosmic chemical evolution (e.g., Malaney & Chaboyer, 1996; Pei, Fall & Hauser, 1999), recent observations indicate at most a mild evolution in DLA global metallicity with redshift for $0 \lesssim z \lesssim 4$ (Prochaska et al. 2003; Khare et al. 2004; Kulkarni, et al., 2005; and references therein). Even theoretical models such as Smoothed-particle-hydrodynamics simulations (Nagamine, Springel, & Hernquist, 2004) predict that the true DLA metallicities could be 1/3 solar at z=2.5 and higher at lower redshifts.

Even at z=2.5, making a census of the predicted and observed neutral comoving densities of gas, Ω, and metals, Ω_Z, one finds that most of the baryons are in the Lyman-α forest but its metal content is extremely low. The measured value of Ω_{HI}(DLA) is only a small fraction of $\Omega_{baryons}$ and the DLA global mean metallicity is about $1/10^{th}$ solar. The metallicity of Lyman break galaxies is still poorly constrained; but, in

any case, these objects are known to be star-forming galaxies and may not be representative of the normal galaxy population. In total, these three components account for no more than $\approx 10 - 15\%$ of what we expect to have been produced by z=2.5 (Pettini et al. 2003; Bouché et al. 2005). The missing metals problem in low-redshift DLAs is even more surprising since the high global star formation rate estimates at z>1.5 (e.g. Madau et al. 1998) imply that higher metallicities should be expected at low redshift.

It is possible that Ω_Z(DLA) has been underestimated. Metal-rich DLAs could obscure quasars due to their possible high dust content (Fall & Pei 1993). This may be the reason for the apparent low metallicity in the DLAs observed in optically selected quasars (e.g., Fall & Pei 1993; Boissé et al. 1998). Recently Vladilo and Péroux (2005) have shown that the fraction of high-redshift DLAs missed due to dust obscuration, could be up to 50%, which is consistent with the results of surveys of radio selected quasars (Ellison et al. 2001). They have estimated that at z~2.3, the real mean metallicity of DLAs could be 5 to 6 times higher than what is observed, which may help alleviate the missing metals problems. Indeed, systems at lower redshift may have significantly more dust at any given metallicity simply because the dust in these objects has had more time to process the elements.

On the other hand, new lines of evidence are pointing toward lower N_{HI} quasar absorbers like Lyman Limit Systems (LLS) and sub-DLAs being more metal-rich (Péroux et al. 2003a; Jenkins et al. 2005). The dust bias, if real, is also likely to be less severe for metal-rich sub-DLAs as compared to the metal-rich DLAs due to the lower gas and therefore dust content in the former, for a constant dust to gas ratio. Thus, the obscuration bias will affect the DLAs at a lower dust-to-gas ratio as compared to the sub-DLAs. This scenario is consistent with the recent radio surveys (e.g., Vladilo & Péroux 2005), but still needs to be further quantified observationally. Indeed, Zn measurements exist for only two sub-DLAs at low z: the marginally super-solar sub-DLA toward Q0058+019 with z_{abs}=0.61, log N_{HI}=20.08, and [Zn/H]=+0.08 (Pettini et al. 2000), and the supersolar sub-DLA toward SDSS J1323−0021 with z_{abs}=0.72, log N_{HI}=20.21, and [Zn/H]=+0.40 (Khare et al. 2004). Although Khare et al. reported [Zn/H]=+0.40 for this latter absorber, the modest resolution of their MMT data could not resolve the Mg I+Zn II λ 2026 and Cr II+Zn II λ 2062 blends.The extent of line saturation on the derived column densities was also unclear. With the goal of addressing these issues with high-resolution data, we obtained VLT/UVES spectra of this quasar, which are presented here. These new data are essential to confidently determine the metallicity by minimising the problem of line saturation. Section 2 presents the observational set-up and data reduction process, while section 3 presents the analysis. Section 4 provides a discussion of the results.

2. Observations and Data Reduction

Spectra of SDSS J1323−0021 (z_{em}=1.390; SDSS mag g = 18.49) were acquired in service mode as Director's Discretionary Time (DDT) on 3$^{\mathrm{rd}}$ of March and 13$^{\mathrm{th}}$ of March

2005 with the high-resolution UVES spectrograph mounted on Kueyen Unit 2 VLT (D'Odorico et al. 2000). Three exposures of length 4100 sec, 3500 sec and 4100 sec were obtained with standard 390+562 settings thus providing a wavelength coverage of ~3300Å-4400Å, 4700Å-5600Å and 5800Å-6600Å.

The data were reduced using the most recent version of the UVES pipeline to accommodate for the new format of the raw fits file (version: uves/2.1.0 flmidas/1.1.0). Master bias and flat images were constructed using calibration frames taken the closest in time to the science frames. The science frames were extracted with the "optimal" option. The spectrum was then corrected to vacuum heliocentric reference. The resulting spectra were combined weighting each spectrum with its signal-to-noise. The final spectra have resolution of 4.7 km s^{-1} at Zn II λ2026. The spectra were divided into 100 Å regions, and each region normalised using cubic spline functions of orders 1 to 5.

3. Analysis

Several lines of Zn II, Cr II, Fe II, Mn II, and Ti II were detected at z_{abs}=0.716. Fe I, Zn I, and Co II were not detected. The column densities were estimated by fitting multi-component Voigt profiles to the observed absorption lines using the program FITS6P (Welty, Hobbs, & York 1991) that evolved from the code used by Vidal-Madjar et al. (1977). FITS6P minimizes the χ^2 between the data and the theoretical Voigt profiles convolved with the instrumental profile. The atomic data were adopted from Morton (2003).

The absorption profiles show a complex velocity structure with a total of 16 components needed. The velocity and Doppler b parameters of the various components were estimated from the Mg I, Mg II, and Fe II lines. The component at 12 km s^{-1} is negligible in most species except Mg I, Zn II and Cr II. The component at 194 km s^{-1} is negligible in all species but Mg II. The component at −121 km s^{-1} is detected in Mg II, Fe II, and Mn II, but not in Mg I, Zn II, Cr II, or Ti II. The best-fit column densities in the individual components and their uncertainties were estimated assuming the same fixed b and v values for all species in a given component (Figure 1). The results of the profile fitting analysis are summarised in Table 1. Column densities in the few weak components that could not be well-constrained due to noise are marked with "..."; their contributions to the total column densities (listed in Table 2) are negligible. As an additional check, we also estimated the total column densities using the apparent optical depth (AOD; Savage & Sembach 1991) method for the various detected lines and obtained results consistent with those from the profile-fitting method. The agreement was within 0.01 dex for Mg I and Mn II, within 0.1 dex for Fe II and Zn II, and within 0.15 dex for Ti II.

The Mg I λ2026.5 contribution to the Zn II λ2026.1 line was estimated using the component parameters for Mg I derived from the Mg I λ2852 profile. This contribution, indicated by a dashed blue curve in the top left panel of Fig 1, was a small fraction of the observed strength of the λ2026 line. The remaining part of the λ2026 line was fitted with a 15-component model for Zn II, using the same b values and velocities, but varying the column densities in the individual components. The

Table 1. Parameter fit to the $z_{abs} = 0.716$ sub-DLA model. Velocities and b are in km s^{-1} and N's are in cm^{-2}.

	Vel	b	Mg I	Mg II	Fe II	Zn II	Cr II	Mn II	Ti II	[Fe/Zn]	[Mn/Fe]
N(X)	−120.8	7.1	...	5.63e12	5.82e12	...	...	3.75e11	...	...	0.79
σ	...	...	...	1.66e11	4.08e11	...	...	1.26e11	...	...	...
N(X)	−96.9	16.3	...	3.65e12	3.64e12	2.32e12	<2.81e12	2.97e11	2.09e11	−2.65	0.89
σ	...	...	...	1.21e11	4.31e11	6.53e11	...	1.93e11	1.27e11	...	...
N(X)	−80.1	6.2	3.16e10	3.55e12	3.92e12	...	<1.69e12	2.09e11	1.86e11	...	0.71
σ	...	...	1.15e10	1.36e11	3.69e11	...	...	1.23e11	8.41e10	...	...
N(X)	−62.9	5.5	1.20e11	8.13e12	4.25e12	<3.10e11	<4.77e11	2.01e11	1.07e11	−1.71	0.65
σ	...	...	1.23e10	3.68e11	4.22e11	...	...	1.01e11	8.00e10	...	...
N(X)	−51.4	5.0	<1.33e10	>2.86e12	5.74e12	<2.56e11	...	1.44e11	<6.92e10	−1.49	0.38
σ	...	...	...	...	1.30e12	...	...	1.19e11	...	...	...
N(X)	−43.0	7.4	4.80e11	>6.01e13	2.41e13	1.07e12	...	1.98e11	1.32e11	−1.49	−0.11
σ	...	...	2.29e10	...	3.54e12	5.18e11	...	1.43e11	9.85e10	...	...
N(X)	−13.0	12.5	3.04e12	>2.38e14	1.97e14	2.57e12	...	2.40e12	4.79e11	−0.96	0.07
σ	...	...	1.48e11	...	2.54e13	6.22e11	...	3.14e11	2.16e11	...	...
N(X)	3.9	30.5	2.36e12	>1.48e14	4.00e14	...	...	5.33e12	<4.17e11	...	0.10
σ	...	...	2.03e11	...	2.63e13	...	...	5.28e11	...	...	...
N(X)	12.0	5.0	1.44e11	...	...	<3.66e11	<3.20e11	...	<3.89e10	...	0.01
σ	...	...	4.81e10	...	...	...	...	...	...	...	...
N(X)	28.3	12.0	2.06e12	>7.14e13	1.15e14	1.53e12	<2.37e12	1.28e12	3.80e11	−0.97	0.03
σ	...	...	1.25e11	...	2.94e13	7.60e11	...	2.86e11	1.53e11	...	...
N(X)	44.5	11.0	4.76e12	>2.30e13	2.89e14	7.76e12	...	4.34e12	4.37e11	−1.27	0.16
σ	...	...	4.37e11	...	5.42e13	1.48e12	...	2.90e11	1.22e11	...	...
N(X)	56.6	6.9	8.70e11	>4.62e13	2.83e13	<2.73e11	...	6.30e11	2.69e11	−0.83	0.33
σ	...	...	1.15e11	...	1.82e13	...	...	1.97e11	9.48e10	...	...
N(X)	71.8	11.9	1.93e12	>5.09e14	3.12e14	2.49e12	6.07e12	3.62e12	1.58e11	−0.75	0.04
σ	...	...	5.19e10	...	4.29e13	7.30e11	3.24e12	2.22e11	1.05e11	...	...
N(X)	92.7	6.4	2.42e12	>2.99e14	3.76e13	7.35e12	<1.54e12	1.20e12	2.09e11	−2.14	0.48
σ	...	...	8.51e10	...	4.70e12	1.49e12	...	1.40e11	7.87e10	...	...
N(X)	119.3	8.0	7.45e10	4.49e12	2.33e12	5.13e11	6.01e12	1.98e11	1.02e08	−2.19	0.91
σ	...	...	1.32e10	4.90e07	2.85e11	4.48e11	3.11e12	1.27e11	1.42e07	...	...
N(X)	194.1	4.6	2.44e10	1.91e12	...	...	...	...	...	...	...
σ	...	...	1.00e10	7.56e10	...	...	...	...	...	...	...

Zn II fit thus obtained was used to estimate the Zn II contribution to the $\lambda2062$ line. The remaining part of the $\lambda2062$ line was fitted with a 15-component model for Cr II, using the same set of b values and velocities. This was the only available estimate for Cr II, since the Cr II $\lambda\lambda$ 2056, 2066 lines lie in noisy regions and are undetected. The relatively large errors in the Cr II column densities arise from the noisy nature of the $\lambda2062$ line. The Fe II column densities in the components at low velocities were constrained by using the Fe II $\lambda\lambda2260, 2374$ lines, since the stronger Fe II lines are saturated. The weaker Fe II components at high positive and negative velocities were constrained in column density using the $\lambda\lambda2374, 2382, 2600$ lines, since these components are poorly constrained by the weaker $\lambda\lambda2260, 2374$ lines. The Mg II $\lambda2796, 2803$ profiles were fitted together, but provide only a lower limit to Mg II owing to saturation in the central components. The relative abundances were calculated using solar abundances from Asplund et al. (2005), adopting the mean of photospheric and meteoritic values for Mg, Ti, Cr, Fe, Zn, and the meteoritic value for Mn.

One concern is that sub-DLAs may be partially ionised in H, artificially enhancing the ratio of Zn II to H I, for instance. To investigate the ionisation corrections, we used the CLOUDY software package (version 94.00, Ferland 1997) and computed photoionisation models assuming ionisation equilibrium and a solar abundance pattern. We thus obtained the theoretical column density predictions for any ionisation state of all observed ions as a function of the ionisation parameter U. Our findings confirm the observations: from a comparison of the observed and theoretical Mg II/Mg I ratios, we deduced that the gas in this sub-DLA is predominantly neutral ($\log U < -5$) and the overall abundance pattern is probably not solar. This latter point is also clear from the relative abundances listed for each component in Table 1. It should be pointed out that there are no third ionisation stage detected in the system under study. Nevertheless, we do have Ti II, which has the same ionisation potential as H I. The fact that Ti is not suppressed compared to Fe or Mn also implies that the gas is neutral with low ionisation parameter.

4. Discussion and Conclusions

Table 2 lists the abundances, using $\log N_{\mathrm{HI}} = 20.21^{+0.21}_{-0.18}$ (Khare et al. 2004) that we derived from Voigt profile fitting of the damped Ly-α line in the publicly available HST/STIS spectrum of SDSS J1323−0021 (program GO 9382; PI: Rao). Rao et al. (2005) obtained $\log N_{\mathrm{HI}} = 20.54^{+0.16}_{-0.15}$ from the same data
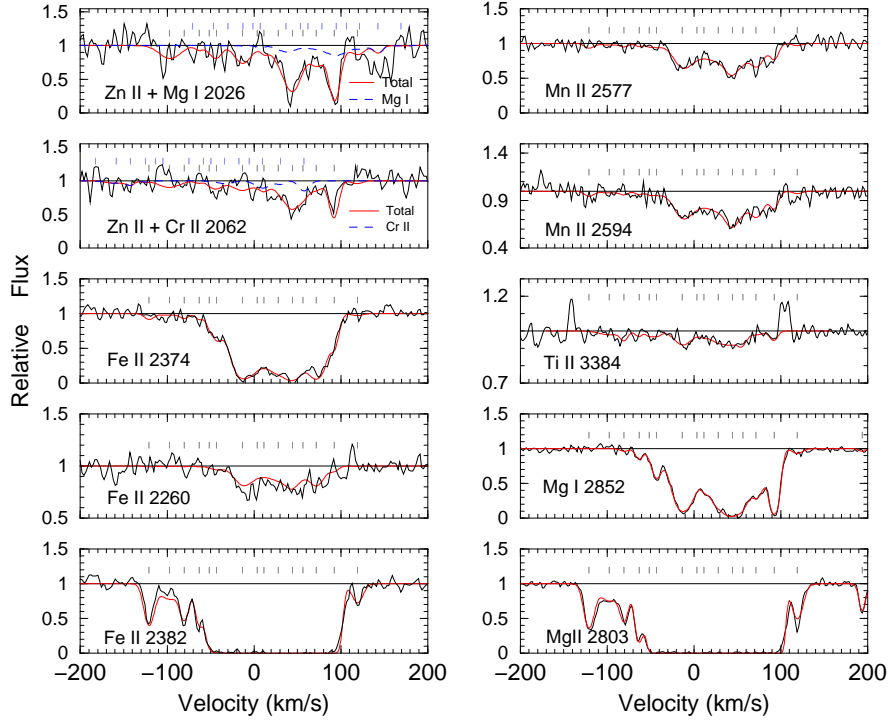
Fig. 1. Velocity plots of some of the element lines detected at z_{abs} = 0.716 toward SDSS J1323−0021. The black tick-marks indicate positions of the components and the red curves denote the best-fit profiles. In the two top left panels, the upper set of blue tickmarks indicate positions of the components of Mg I λ2026 and Cr II λ2062, respectively, whilst the blue curves show their contributions to the absorption profiles. Note that different ordinates are used on the sub-frames.

Table 2. Summary of total abundances.

Id	$\log N_{total}$	$A(X/N)_{\odot}$	$[X/H]^*$
Mg I	13.26 ± 0.01	...	...
Mg II	> 15.15	-4.47	> -0.58
Fe II	15.15 ± 0.03	-4.55	-0.51 ± 0.20
Zn II	13.43 ± 0.05	-7.40	$+0.61 \pm 0.20$
Cr II	< 13.33	-6.37	< -0.52
Mn II	13.31 ± 0.02	-6.53	-0.37 ± 0.20
Ti II	12.49 ± 0.11	-7.11	-0.61 ± 0.22

* The error bars on [X/H] include the errors in $\log N(X)$ and $\log N_{HI}$.

set. We use the former value since it gives a smaller residual with respect to the data and therefore regard this absorber as a sub-DLA. For either N_{HI}, the strength of the Zn II lines detected in our UVES spectrum implies a super-solar metallicity. Using the standard definition: $[X/H] = \log[N(X)/N(H)]_{DLA} - \log[N(X)/N(H)]_{\odot}$, we find [Zn/H]=+0.61.

In principle, if Mg I λ 2852 were substantially saturated, the contribution of Mg I λ 2026 could be higher than our best-fit estimate. However, based on our apparent optical depth measurements and profile-fitting results, we estimate that it would take ∼8 times more total Mg I than the value derived from the λ2852 line to contribute the entirely of the λ2026 line. Such a high value of Mg I can be ruled out by the observed profile of the λ2852 line. (Of course, such a scenario would also be inconsistent with the observed strength and profile of the λ2062 line.) To understand this issue in more detail, we estimated the

maximum Mg I in the dominant components that would still give the shape of the Mg I λ2852 profile consistent with the observed profile within the noise level in the continuum. This maximum total Mg I = $2.7e13$ is about 50% larger than the best-fit value listed in Table 2. Putting this maximum Mg I model in the λ2026 line, the corresponding total Zn II needed to fit the remaining part of the λ 2026 line would be 2.5e13, lower by < 10% from our best-fit value. Thus [Zn/H] is at least > +0.59, indicating that our result would not be affected much by saturation of Mg I λ 2852. Finally, as an additional check, we also estimated the maximum contribution of Cr II 2062 by rebinning our spectrum by factors of 10 or 20, measuring the upper limit for Cr IIλ 2056 in the rebinned spectrum. We then spread this upper limit for N(Cr II) over the 2062 profile, using the velocity model derived from the combination of the lines. We assume the same Fe/Cr ratio in all components, taking the percentage of Cr II in each components relative to total N(CrII) summed over all components to be the same as the corresponding percentage of Fe II in that component. Fitting the remaining part of the λ2062 line with a 15-component model of Zn II, we estimated $N_{ZnII} > 2.05e13$, i.e. $[Zn/H] > 0.50$.

The abundances of Fe, Cr, Mn, and Ti lie in the range of −0.4 to −0.6 dex, and indicate that this absorber is not only metal-rich, but also very dusty. Using the model from Vladilo (2004), we find that 95% of the Fe is in dust phase and the total metallicity is even slightly higher than 0.6 dex. This sightline also shows substantial reddening compared to the SDSS quasar composite ($\Delta(g - i)$ = 0.47; Khare et al. 2004). Considering

only the better-determined components between -13 and 100 km s^{-1}, Fe/Zn varies by a factor of ~ 3 and Ti/Zn varies by ~ 35. [Mn/Fe] varies by ~ 3, but indicates a super-solar Mn abundance with respect to Fe in all components. The relative abundance of Mn with respect to Fe is not expected to exceed the solar value as Mn, unlike Fe, has an odd atomic number. However, [Mn/Fe]>0 is often seen in the Galactic interstellar gas due to the stronger depletion of Fe on to dust grains.

To summarise, our high resolution VLT/UVES data have allowed us to alleviate the saturation issue in Zn II and Cr II lines and therefore unambiguously prove the super-solar metallicity of the sub-DLA at z_{abs}=0.716 toward SDSS J1323$-$0021. If the dust obscuration bias for DLAs is indeed significant, as proposed by Vladilo and Péroux (2005), sub-DLA systems such as the one reported here could be better probes of dusty regions with significant past star formation (e.g. Lauroesch et al. 1996; York et al. 2006), as similar DLA systems will be missed due to dust obscuration. On the other hand, it is also, possible to envisage a scenario where the dust obscuration is not very significant in quasar absorbers (as is indicated by the rising spectrum of gamma-ray burst afterglows). In this scenario it is possible that the sub-DLA systems may indeed be more metal-rich as compared to DLAs as indicated by observations of Péroux et al. (2003a) and by the observations of super-solar metallicity in such systems presented here and in Pettini et al (2003). With the large-scale spectroscopic surveys of quasars currently underway (e.g. the SDSS, York et al. 2000, York et al. 2001), such metal-rich sub-DLA systems may be found in large numbers. If future observations indeed find such systems, sub-DLAs may contribute significantly to the overall global metallicity.

References

Asplund, M., Grevesse, N. & Sauval, A. J., ASP Conference Series, 2005. Ed Bash & Barnes, 336, 25.

Bouché, N., Lehnert, M. D. & Péroux, C., 2005, MNRAS, 364, 319.

Boissé, P., Le Brun, V., Bergeron, J. & Deharveng, J-M., 1998, 1998, A&A, 333, 841.

D'Odorico, S., Cristiani, S., Dekker, H., Hill, V., Kaufer, A., Kim, T. & Primas, F., 2000, SPIE, 4005, 121

Ellison, S. L., Yan, L., Hook, I. M., Pettini, M., Wall, J. V. & Shaver, P., 2001, A&A, 379, 393.

Fall, M. & Pei, Y., 1993, ApJ, 402, 479.

Ferland, G.J., 1997, Hazy, a brief introduction to CLOUDY

Jenkins, E. B., Bowen, D. V., Tripp, T. M. & Sembach, K. R., 2005, ApJ, 623, 767.

Khare, P., Kulkarni, V. P., Lauroesch, J. T., York, D. G., Crotts, A. P. S. & Nakamura, O., 2004, ApJ, 616, 86.

Kulkarni, V. P., Fall, S. M. & Truran, J. W., 1997, ApJ, 484, L7.

Kulkarni, V. P. & Fall, S. M., 2002, ApJ, 580, 732.

Kulkarni, V. P., Fall, S. M., Lauroesch, J. T., York, D. G., Welty, D. E., Khare, P. & Truran, J. W., 2005, ApJ, 618, 68.

Lauroesch, J. T., Truran, J. W., Welty, D. E. & York, D. G., 1996, PASP, 108, 641.

Madau, P., Pozzetti, L. & Dickinson, M., 1998, ApJ, 498, 106.

Malaney. R. A. & Chaboyer, B., 1996, ApJ, 462, 57.

Morton, D. C. 2003, ApJS, 149, 205.

Nagamine, K., Springel, V. & Hernquist, L., 2004, MNRAS, 348, 435.

Pei, Y. C., Fall, S. M. & Hauser, M. G., 1999, ApJ, 522, 604.

Péroux, C., McMahon, R., Storrie-Lombardi, L., & Irwin, M., 2003a, MNRAS, 346, 1103.

Péroux, C., Dessauges-Zavadsky, M., D'Odorico, S., Kim, T. S. & McMahon, R., 2003b, MNRAS, 345, 480.

Péroux, C., Petitjean, P., Aracil, B. & Srianand, A., 2002, New A., 7, 577.

Pettini, M., King, D. L., Smith, L. J. & Hunstead, R. W., 1997, ApJ, 478, 536.

Pettini, M., Ellison, S. L., Steidel, C. C. & Bowen, D. V., 1999, ApJ, 510, 576.

Pettini, M., 2003, XIII Canary Islands Winter School, ed Esteban, López, Herrero, Sánchez.

Pettini, M., Ellison, S. L., Steidel, C. C., Shapley, A. E. & Bowen, D. V., 2000, ApJ, 532, 65.

Prochaska, J., Gawiser, E., Wolfe, A. M., Castro, S. & Djorgovski, S. G., 2003, ApJ, 595L, 9.

Rao, S. M., Turnshek, D. A., & Nestor D. B. 2005, ApJ, 129, 9.

Rao, S. M., Turnshek, D. A., & Nestor D. B. 2005 *in press*.

Savage, B. D. & Sembach, K. R., 1991, ApJ, 379, 245.

Storrie-Lombardi, L. & Wolfe, A., 2000, ApJ, 543, 552.

Vidal-Madjar, A., Laurent, C., Bonnet, R. M., & York, D. G. 1977, ApJ, 211, 91.

Vladilo, G., 2004, A&A, 421, 479.

Vladilo, G. & Péroux, C., 2005, A&A, 444, 461.

Welty, D. E., Hobbs, L. M., & York, D. G. 1991, ApJS, 75, 425.

York, D. G. and the SDSS Collaboration, 2000, AJ, 120, 1579.

York, D. G. and the SDSS Collaboration, 2001, BAAS, 198, 78.05.

York, D. G. et al., 2006, *in preparation*.